articles

molecular pharmaceutics

An Imaging-Driven Model for Liposomal Stability and Circulation

Shengping Qin,[†,‡] Jai Woong Seo,[†,‡] Hua Zhang,[†] Jinyi Qi,[†] Fitz-Roy E. Curry,[§] and Katherine W. Ferrara*[,†]

Department of Biomedical Engineering, University of California, 451 East Health Sciences Drive, Davis, California 95616, and Department of Physiology and Membrane Biology, School of Medicine, University of California, One Shields Avenue, Davis, California 95616

Received April 30, 2009; Revised Manuscript Received July 13, 2009; Accepted July 21, 2009

Abstract: Simultaneous labeling of the drug compartment and shell of delivery vehicles with optical and positron emission tomography (PET) probes is developed and employed to inform a hybrid physiologically based pharmacokinetic model. Based on time-dependent estimates of the concentration of these tracers within the blood pool, reticuloendothelial system (RES) and tumor interstitium, we compare the stability and circulation of long-circulating and temperature-sensitive liposomes. We find that rates of transport to the RES for long-circulating and temperature-sensitive particles are 0.046 and 0.19 h^{-1}, respectively. Without the application of exogenous heat, the rates of release from the long-circulating and temperature-sensitive particles circulating within the blood pool are 0.003 and 0.2 h^{-1}, respectively. Prolonged lifetime in circulation and slow drug release from liposomes result in a significantly greater drug area under the curve for the long-circulating particles. Future studies will couple these intrinsic parameters with exogenous heat-based release. Finally, we develop a transport constant for the transport of liposomes from the blood pool to the tumor interstitium, which is on the order of 0.01 h^{-1} for the Met-1 tumor system.

Keywords: Pharmacokinetic model; imaging-driven model; liposomal stability

Introduction

The development of activatable drug delivery strategies requires co-optimization of the vehicles and the activation strategy. Ideally, the plasma stability of the particle, the release of the drug produced by exogenous energy and the accumulation of particles within the interstitium and reticuloendothelial system should be estimated as a function of time. Positron emission tomography (PET) is a promising noninvasive imaging method to quantify the pharmacokinetics (PK) of radionuclide-labeled particles and drugs in real time. Using PET, the time-dependent concentration within the blood pool, liver and tumor interstitium can be estimated and PK parameters can be quantified, enabling comparisons in which each subject can serve as its own control.[1]

Long-circulating liposomes (LCL) with a polyethylene glycol (PEG) coating circulate for tens of hours and accumulate within tumors over time.[2,3] Despite increased drug levels at the target site with the injection of encapsulated drug as compared with free drug, therapeutic efficacy has

* To whom correspondence should be addressed. Mailing address: University of California, Davis, Department of Biomedical Engineering, 451 East Health Sciences Drive, Davis, CA 95616. Tel: 530-754-9436. Fax: (530)754-5739. E-mail: kwferrara@ucdavis.edu.

† Department of Biomedical Engineering.

‡ These authors contributed equally to this manuscript.

§ Department of Physiology and Membrane Biology, School of Medicine.

(1) Tashjian, J. A.; Dewhirst, M. W.; Needham, D.; Viglianti, B. L. Rationale for and measurement of liposomal drug delivery with hyperthermia using non-invasive imaging techniques. *Int. J. Hyperthermia* **2008**, *24* (1), 79–90.

(2) Senior, J.; Delgado, C.; Fisher, D.; Tilcock, C.; Gregoriadis, G. Influence of Surface Hydrophilicity of Liposomes on Their Interaction with Plasma-Protein and Clearance from the Circulation - Studies with Poly(Ethylene Glycol)-Coated Vesicles. *Biochim. Biophys. Acta* **1991**, *1062* (1), 77–82.

10.1021/mp900122j
Published on Web 07/21/2009

only been modestly improved by pegylated particles,[4−7] presumably because therapeutic efficacy requires the release of the drug or cellular internalization of the particle.[8−10] Temperature-sensitive liposomes (TSL), which show drug release at 39−40 °C, have been demonstrated to increase the drug concentration in tumor interstitium compared with free drug; however, current particles are leaky during prolonged circulation.[11−13]

Our goal was to simultaneously observe the liposomal shell and cargo. To accomplish this, we label the liposomal surface via covalent conjugation of a chelator for ^{64}Cu (12.7 h half-life)[14] and load a hydrophilic near-infrared dye, SIDA,[15,16] with a partition coefficient of −2.3 (similar to hydrophilic drugs such as cisplatin (−2.19)[17]) in the liposomal core. Using PET, the time-dependent concentration of the labeled shell within the blood pool, reticuloendothelial system (RES) and tumor interstitium is estimated. By combining the analyses of PET and optical data, the circulation of the cargo is compared with that of the shell and thus the integrity of the particle can be assessed.

In drug design, pharmacokinetic models are applied to describe drug absorption, distribution and elimination.[18−21] The conventional compartmental pharmacokinetic models[19,22] use one, two or three compartments to describe complex drug transport. Pharmacokinetic parameters that provide the "best fit" of the experimental concentration−time profile are selected. Since the commonly used compartmental pharmacokinetic models lack anatomic or physiologic relevance, the obtained parameters cannot be extrapolated beyond the available experimental data. In contrast, physiologically based pharmacokinetic (PBPK) models map the mass transport scheme into physiologically relevant compartments based on anatomic or physiologic data. Thus, predictions of drug transport in one mammalian species can be applied to data from another species by substituting related physiologic and pharmacokinetic parameters.[20,23,24] Here, we propose a hybrid PBPK model to combine the characteristics of compartmental models and physiologically based models in a subset of organs while other tissues are lumped into the peripheral (tissue) compartment. We validate our hybrid PBPK model by comparing a cholesterol-rich, long-circulat-

(3) Allen, T. M. The Use of Glycolipids and Hydrophilic Polymers in Avoiding Rapid Uptake of Liposomes by the Mononuclear Phagocyte System. *Adv. Drug Delivery Rev.* **1994**, *13* (3), 285–309.

(4) Garcia, A. A.; Kempf, R. A.; Rogers, M.; Muggia, F. M. A phase II study of Doxil (liposomal doxorubicin): Lack of activity in poor prognosis soft tissue sarcomas. *Ann. Oncol.* **1998**, *9* (10), 1131–1133.

(5) Ellerhorst, J. A.; Bedikian, A.; Ring, S.; Buzaid, A. C.; Eton, O.; Legha, S. S. Phase II trial of doxil for patients with metastatic melanoma refractory to frontline therapy. *Oncol. Rep.* **1999**, *6* (5), 1097–1099.

(6) Chidiac, T.; Budd, G. T.; Pelley, R.; Sandstrom, K.; McLain, D.; Elson, P.; Crownover, R.; Marks, K.; Muschler, G.; Joyce, M.; Zehr, R.; Bukowski, R. Phase II trial of liposomal doxorubicin (Doxil (R)) in advanced soft tissue sarcomas. *Invest. New Drugs* **2000**, *18* (3), 253–259.

(7) Halford, S.; Yip, D.; Karapetis, C. S.; Strickland, A. H.; Steger, A.; Khawaja, H. T.; Harper, P. G. A phase II study evaluating the tolerability and efficacy of CAELYX (liposomal doxorubicin, Doxil) in the treatment of unresectable pancreatic carcinoma. *Ann. Oncol.* **2001**, *12* (10), 1399–1402.

(8) Drummond, D. C.; Meyer, O.; Hong, K. L.; Kirpotin, D. B.; Papahadjopoulos, D. Optimizing liposomes for delivery of chemotherapeutic agents to solid tumors. *Pharmacol. Rev.* **1999**, *51* (4), 691–743.

(9) Hauck, M. L.; Larue, S. M.; Petros, W. P.; Poulson, J. M.; Yu, D. H.; Spasojevic, I.; Pruitt, A. F.; Klein, A.; Case, B.; Thrall, D. E.; Needha, D.; Dewhirst, M. W. Phase I trial of doxorubicin-containing low temperature sensitive liposomes in spontaneous canine tumors. *Clin. Cancer Res.* **2006**, *12* (13), 4004–4010.

(10) Lim, H. J.; Masin, D.; McIntosh, N. L.; Madden, T. D.; Bally, M. B. Role of drug release and liposome-mediated drug delivery in governing the therapeutic activity of liposomal mitoxantrone used to treat human A431 and LS180 solid tumors. *J. Pharmacol. Exp. Ther.* **2000**, *292* (1), 337–345.

(11) Kong, G.; Dewhirst, M. W. Hyperthermia and liposomes. *Int. J. Hyperthermia* **1999**, *15* (5), 345–370.

(12) Kong, G.; Anyarambhatla, G.; Petros, W. P.; Braun, R. D.; Colvin, O. M.; Needham, D.; Dewhirst, M. W. Efficacy of liposomes and hyperthermia in a human tumor xenograft model: Importance of triggered drug release. *Cancer Res.* **2000**, *60* (24), 6950–6957.

(13) Needham, D.; Dewhirst, M. W. The development and testing of a new temperature-sensitive drug delivery system for the treatment of solid tumors. *Adv. Drug Delivery Rev.* **2001**, *53* (3), 285–305.

(14) Seo, J. W.; Zhang, H.; Kukis, D. L.; Meares, C. F.; Ferrara, K. W. A Novel Method to Label Preformed Liposomes with ^{64}Cu for Positron Emission Tomography (PET) Imaging. *Bioconjugate Chem.* **2008**, *19* (12), 2577–2584.

(15) Terpetschnig, E.; Szmacinski, H.; Ozinskas, A.; Lakowicz, J. R. Synthesis of squaraine-N-hydroxysuccinimide esters and their biological application as long-wavelength fluorescent labels. *Anal. Biochem.* **1994**, *217* (2), 197–204.

(16) Licha, K.; Riefke, B.; Ntziachristos, V.; Becker, A.; Chance, B.; Semmler, W. Hydrophilic cyanine dyes as contrast agents for near-infrared tumor imaging: synthesis, photophysical properties and spectroscopic in vivo characterization. *Photochem. Photobiol.* **2000**, *72* (3), 392–8.

(17) Long, D. F.; Repta, A. J. Cisplatin: chemistry, distribution and biotransformation. *Biopharm. Drug Dispos.* **1981**, *2* (1), 1–16.

(18) El-Kareh, A. W.; Secomb, T. W. Theoretical models for drug delivery to solid tumors. *Crit. Rev. Biomed. Eng.* **1997**, *25* (6), 503–571.

(19) Strand, S. E.; Zanzonico, P.; Johnson, T. K. Pharmacokinetic Modeling. *Med. Phys.* **1993**, *20* (2), 515–527.

(20) Gerlowski, L. E.; Jain, R. K. Physiologically Based Pharmacokinetic Modeling - Principles and Applications. *J. Pharm. Sci.* **1983**, *72* (10), 1103–1127.

(21) Himmelstein, K. J.; Lutz, R. J. Review of the Applications of Physiologically Based Pharmacokinetic Modeling. *J. Pharmacokinet. Biopharm.* **1979**, *7* (2), 127–145.

(22) Watabe, H.; Ikoma, Y.; Kimura, Y.; Naganawa, M.; Shidahara, M. PET kinetic analysis - compartmental model. *Ann. Nucl. Med.* **2006**, *20* (9), 583–588.

(23) Nestorov, I. Whole-body physiologically based pharmacokinetic models. *Expert Opin. Drug Metab. Toxicol.* **2007**, *3* (2), 235–249.

(24) Hu, L. J.; Au, J. L. S.; Wientjes, M. G. Computational modeling to predict effect of treatment schedule on drug delivery to prostate in humans. *Clin. Cancer Res.* **2007**, *13* (4), 1278–1287.

ing particle with a temperature-sensitive particle that incorporates a lysolipid and estimating key parameters.

Microvascular permeability has been shown to vary with molecular weight and tumor type, limiting the rate of extravasation.[25−27] While four coefficients describe microvascular permeability to water and small solutes in normal tissue (the hydraulic permeability, the diffusional permeability, the ultrafiltration coefficient and the osmotic reflection coefficient), microvascular permeability to macromolecules is dominated by microfluidic convection and diffusion.[27−29] Classical studies of vascular permeability have typically required the injection of multiple tracers, together with invasive procedures.[27,30] Using modern imaging technologies such as MR imaging, contrast-enhanced computed tomography and optical fluorescence, imaging-based data enable quantitative measurement of vascular permeability.[28,30−34] Although the concept of compartment has been incorporated, previous analyses use empirical data-fitting and mass conservation is not enforced. A model which is based on whole-body mass conservation is needed to predict the liposome and drug concentration over time and thus vascular permeability in each region of interest.[24,35,36] Here, microvascular permeability is predicted in an intact system, facilitating translational studies of various macromolecular and nanoparticle therapies.

Materials and Methods

Materials. $^{64}CuCl_2$ was purchased from Trace life Science (Denton, TX). Chemicals for the synthesis of SIDA were purchased from Sigma-Aldrich (St. Louis, MO). Solvents were purchased from EMD (Gibbstown, NJ) or Sigma-Aldrich (St. Louis, MO) as HPLC grade. Phosphate-buffered saline (PBS, 1×) was purchased from Invitrogen (Carlsbad, CA). All lipids and a miniextruder were purchased from Avanti Polar Lipids (Alabaster, AL). All eppendorf tubes and glassware for labeling were prewashed with absolute ethanol and acetone and dried in an oven before use.

Synthesis. Bis-1,1′-(4-sulfobutyl)indotricarbocyanine-5,5′-dicarboxylic Acid (SIDA). SIDA was synthesized from hydrazinobenzoic acid in three steps using a previously reported method[15,16] with an overall yield of 47%. The product was characterized by ^{1}H NMR and electron spray ionization mass spectrometry (ESI). The emission maximum wavelength of SIDA in PBS (pH 7.0) was 789 nm.

Preparation of Dual Labeled Liposomes. Benzyl-TETA (6-[*p*-(bromoacetamido)benzyl]-1,4,8,11-tetraazacyclotetradecane-*N*,*N*′,*N*″,*N*‴-tetraacetic acid) (BAT), which selectively forms a stable complex with Cu(II), was used as the chelator for ^{64}Cu.[14] Using solid phase synthesis, BAT was conjugated to a distearoyl lipid (with PEG-1200 as a stable linker) for insertion within the liposomal membrane.[14] Accordingly, we modified the previously reported ^{64}Cu labeling procedure in order to accommodate dual labeling of the shell and core. Lipid mixtures for temperature-sensitive liposomes (TSL, 10 mg, DPPC:MPPC:DSPE-PEG2K:BAT lipid = 85.9:10:4:0.1, mol/mol/mol/mol) and long-circulating liposomes (LCL, 10 mg, HSPC:cholesterol:DSPE-PEG2K:BAT lipid = 55.9:39:5:0.1, mol/mol/mol/mol) were dried by nitrogen gas with vortexing to create a thin film, which was further dried under vacuum overnight to completely remove chloroform. The dried lipid thin film was suspended in 0.125 mM SIDA solution (0.4 mL) in 0.125 M ammonium acetate buffer (pH 5.5) or 0.10 M ammonium citrate buffer (pH 5.5). The lipid solution was incubated for 5−10 min at 60 °C to suspend the thin lipid film into the SIDA solution. After sonication for several seconds, lipid mixtures were drawn up into a 1 mL syringe for extrusion. Lipids were passed 21 times through a 100 nm membrane filter (Whatman, NJ) at 60−62 °C on a heating block to load the SIDA passively in the core of the liposome. Freshly prepared liposomes filled with

(25) Aukland, K.; Reed, R. K. Interstitial-Lymphatic Mechanisms in the Control of Extracellular Fluid Volume. *Physiol. Rev.* **1993**, *73* (1), 1–78.
(26) Michel, C. C. Transport of macromolecules through microvascular walls. *Cardiovasc. Res.* **1996**, *32* (4), 644–653.
(27) Michel, C. C.; Curry, F. E. Microvascular permeability. *Physiol. Rev.* **1999**, *79* (3), 703–761.
(28) Dreher, M. R.; Liu, W. G.; Michelich, C. R.; Dewhirst, M. W.; Yuan, F.; Chilkoti, A. Tumor vascular permeability, accumulation, and penetration of macromolecular drug carriers. *J. Natl. Cancer Inst.* **2006**, *98* (5), 335–344.
(29) Rippe, B.; Haraldsson, B. Transport of Macromolecules across Microvascular Walls - the 2-Pore Theory. *Physiol. Rev.* **1994**, *74* (1), 163–219.
(30) Pollard, R. E.; Garcia, T. C.; Stieger, S. M.; Ferrara, K. W.; Sadlowski, A. R.; Wisner, E. R. Quantitative evaluation of perfusion and permeability of peripheral tumors using contrast-enhanced computed tomography. *Invest. Radiol.* **2004**, *39* (6), 340–349.
(31) Kruger, E. F.; Puchalski, S. M.; Pollard, R. E.; Galuppo, L. D.; Hornof, W. J.; Wisner, E. R. Measurement of equine laminar blood flow and vascular permeability by use of dynamic contrast-enhanced computed tomography. *Am. J. Vet. Res.* **2008**, *69* (3), 371–377.
(32) Uematsu, H.; Maeda, M.; Sadato, N.; Matsuda, T.; Ishimori, Y.; Koshimoto, Y.; Yamada, H.; Kimura, H.; Kawamura, Y.; Matsuda, T.; Hayashi, N.; Yonekura, Y.; Ishii, Y. Vascular permeability: Quantitative measurement with double-echo dynamic MR imaging - Theory and clinical application. *Radiology* **2000**, *214* (3), 912–917.
(33) Watanabe, K.; Nakagawa, H.; Tsurufuji, S. A New Sensitive Fluorometric Method for Measurement of Vascular-Permeability. *J. Pharmacol. Methods* **1984**, *11* (3), 167–176.
(34) Tozer, G. M.; Prise, V. E.; Wilson, J.; Cemazar, M.; Shan, S. Q.; Dewhirst, M. W.; Barber, P. R.; Vojnovic, B.; Chaplin, D. J. Mechanisms associated with tumor vascular shut-down induced by combretastatin A-4 phosphate: Intravital microscopy and measurement of vascular permeability. *Cancer Res.* **2001**, *61* (17), 6413–6422.
(35) Tsuchihashi, M.; Harashima, H.; Kiwada, H. Development of a pharmacokinetic/pharmacodynamic (PK/PD)-simulation system for doxorubicin in long circulating liposomes in mice using peritoneal P388. *J. Controlled Release* **1999**, *61* (1−2), 9–19.
(36) Aarons, L. Physiologically based pharmacokinetic modelling: a sound mechanistic basis is needed. *Br. J. Clin. Pharmacol.* **2005**, *60* (6), 581–583.

SIDA solution and incubated within a SIDA solution were cooled to room temperature. This liposomal solution was incubated with $^{64}CuCl_2$ (Trace life science, CA), buffered with 0.1 M ammonium citrate solution (pH 5.5, 0.05 mL), for 40 min at 30 °C to create a stable complex with BAT on the liposomal surface.[14] Nonspecific binding of ^{64}Cu was removed by adding 0.1 M EDTA solution and incubating for 10 min. The dual-labeled liposome mixture was eluted through a size exclusion column (Sephadex-G75, GE Healthcare) preconditioned with PBS buffer in order to remove free SIDA and free ^{64}Cu. Radiochemical purities of purified liposomes, measured with radio-TLC (thin layer chromatography), exceeded 98%. After the radioactivity decayed, the size was measured with a NICOMP 380 ZLS (Particle Sizing Systems, Santa Barbara, CA), where the diameter of the liposomes was $\sim 100 \pm 15$ nm.

***In Vitro* Liposomal Stability in PBS.** For an *in vitro* study of stability, both TSL and LCL were prepared as described above; however, the concentration of SIDA was increased to a 5 mM solution, resulting in a self-quenched dye. Isolated liposomes (0.05 mg in 10 μL of PBS) were added to PBS (0.5 mL). Liposomal solution (0.1 mL per well) was transferred to the 98 well plate, and the fluorescence ($\lambda_{em} =$ 789 nm, $\lambda_{ex} = 754$ nm) was read at several time points over 24 h. The percent release was calculated by normalizing the fluorescence reads by the maximum fluorescence obtained after breaking the liposomes with 10% TRITON X-100 solution (10 μL). Below 37 °C in PBS, there was no significant release of SIDA (<3%) in either case.

***In Vivo* Pharmacokinetic Study with Met-1 Mouse Model.** All animal studies were conducted under a protocol approved by the University of California, Davis Animal Use and Care Committee. A total of 8 animals (female FVB mice, 6−10 weeks, 15−25 g, Charles River, MA) were examined over the course of this study. Met-1 tumors were transplanted 19 days prior to liposome injection and imaging. Mice were anesthetized with 3.5% isofluorane, maintained at 2.0−2.5% isofluorane and catheterized to ensure proper tail vein injection. Liposomes (~1 mg/mouse, 110−400 μCi/mouse) were manually injected over 15 s, with two mice scanned at one time on a bed. PET and optical data were collected over 48 h at multiple time points (0 h, 6 h, 18 h, 28 h, and 48 h). PET scans were performed on a microPET Focus scanner (Siemens Preclinical Solutions, Inc., Knoxville, TN) with a scan duration of 30 min, and the PET images were reconstructed using the filtered back projection (FBP) algorithms and each organ of interest was manually segmented using ASIPro software (Siemens Preclinical Solutions, Inc.). Region-of-interest (ROI) analysis results, after time-decay correction, are expressed as percentage of injected dose per cubic centimeter (% ID/cm^3) for organs of interest. Fluorescence images were acquired with the IVIS Xenogen system (Xenogen Corp., Alameda, CA), and analyzed with Living Image software 2.5 (Xenogen Corp.). Specifically, the system settings were as follows: binning = 4, exposure time = 5 s, field-of-view = 15, f-stop = 2, filters with an excitation of 705−780 nm and emission of 810−885 nm, and the bed temperature at 37 °C. The images were displayed in terms of "efficiency", where the fluorescence emission signals are normalized to the incident excitation intensity to eliminate the variable excitation light from the measurement and enable a more quantitative comparison of fluorescent signals. The images were quantified by ROI analysis.

Imaging-Driven Pharmacokinetic Model

Our goal is to develop a real-time formalism to characterize nanoparticle stability and pharmacokinetics by using PET to label the shell and fluorescence imaging techniques to label the drug compartment. PET images of particles include two components: radioactivity from within a blood vessel and the extravascular activity resulting from extravasation or uptake. The image intensity at time t can be expressed as

$$I_i^P(t) = \eta_i I_B^P(t) + (1 - \eta_i) I_{Si}^P(t) \tag{1}$$

where I is the image intensity. The superscript P refers to the PET data, the subscripts B and S refer to imaging components from the plasma and organ interstitium and the subscript i refers to the organ index ($i = 2$ for tissue and $i = 3$ for tumor). η_i is an estimate of the plasma volume fraction for a specific organ, which is calculated using the PET intensity at time zero.

$$\eta_i = \frac{I_{Si}^P(0)}{I_B^P(0)} \tag{2}$$

We present the PET intensity within the liver, which is representative of the kinetics of uptake and clearance from the RES. The liposomes and lipid metabolites are primarily transported within the plasma components and we denote the PET intensity of the radiolabeled liposomes and lipid metabolites in the blood pool (i.e. plasma) by I_L^P and $I_{L_5}^P$, Figure 2(a). The total PET intensity in plasma can be described as

$$I_B^P(t) = I_L^P(t) + I_{L_5}^P(t) \tag{3}$$

Let $B^P(t)$, $T^P(t)$, $L^P(t)$ indicate the plasma, tumor and liver PET measurements (% ID/cm^3) as a function of time. Equations 3 and 1 lead to

$$\begin{aligned} B^P(t) &= C_L(t) + C_{L_5}(t) \\ T^P(t) &= \eta_T B^P(t) + (1 - \eta_T) C_{L_3}(t), \quad \eta_T = \frac{T^P(0)}{B^P(0)} \\ L^P(t) &= \eta_L B^P(t) + (1 - \eta_L) C_{L_4}(t), \quad \eta_L = \frac{L^P(0)}{B^P(0)} \end{aligned} \tag{4}$$

Notation is defined in the caption of Figure 2.

After the intravenous bolus injection, the optical probe circulates encapsulated within particles and as free fluorophore. The optical image intensity in plasma can be expressed in the following equation:

$$I_B^O(t) = I_{B_F}^O(t) + I_{B_E}^O(t) \quad (5)$$

where the subscripts F and E denote the free and encapsulated fluorophore. As in ref 37, we find that the fluorescence intensity is proportional to the probe concentration *in vivo* with a low concentration of probe within the particles and of the particles within the vasculature or tissue (<125 μM). Therefore, eq 5 can be expressed in terms of the normalized probe concentrations in plasma as

$$B^O(t) = C_F(t) + C_E(t) \quad (6)$$

where $B^O(t)$ and the corresponding C's are nondimensional and describe the normalized, background-subtracted optical intensity from regions of interest. Equation 6 was used to predict the time variation in the optical efficiency in plasma based on measurements of superficial fluorescence.

In order to evaluate liposome stability and accumulation in the tumor, a hybrid PBPK model was devised; see Figure

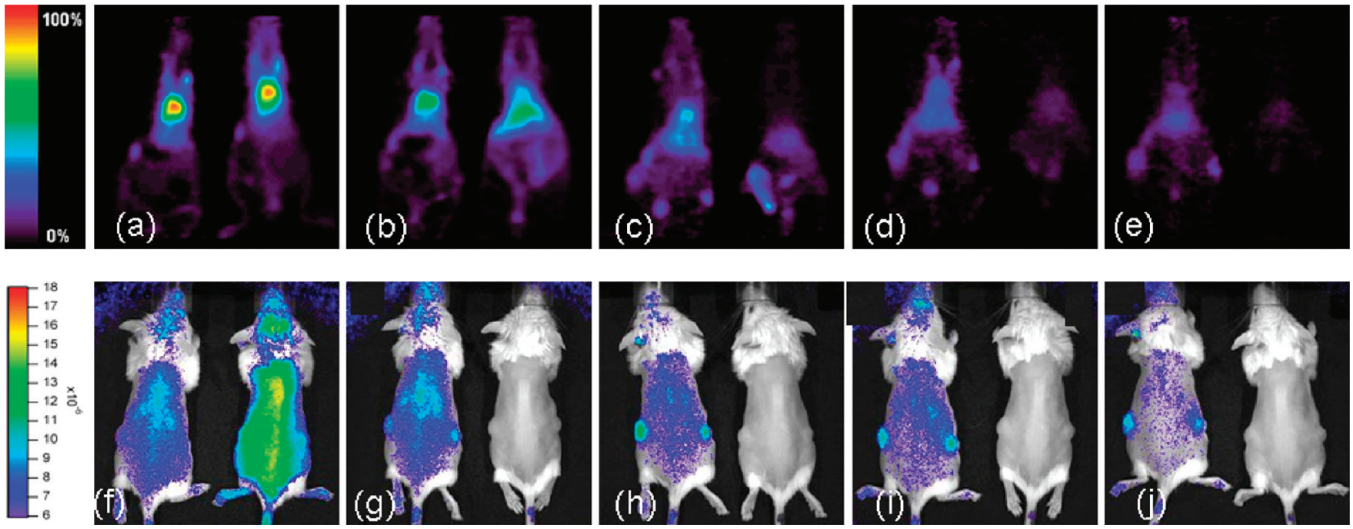

Figure 1. Micro-PET (a-e) and fluorescent (f-j) images acquired after injection of radiolabeled (^{64}Cu) liposomes encapsulating a fluorescent dye (SIDA). Images acquired at time after administration: (a) and (f) 0 h, (b) and (g) 6 h, (c) and (h) 18 h, (d) and (i) 28 h, (e) and (j) 48 h. Left mouse was injected with LCL and right mouse with TSL.

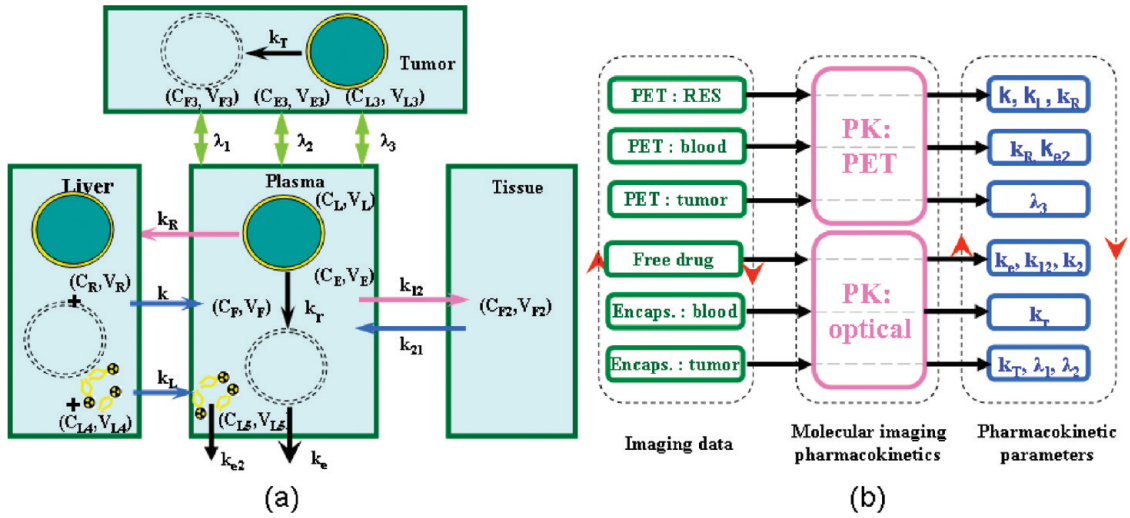

Figure 2. (a) Illustration of the hybrid PBPK model. *C* denotes concentration, *V* denotes distribution volume, subscript F denotes free dye, subscript E denotes encapsulated (abbreviated as Encaps. in Figure) dye and subscript L denotes liposomes. The concentration and distribution volume of the drug in the liver are C_R, V_R; those of the PET probe (liposome, lipid, and metabolites) in the liver are C_{L4}, V_{L4}; and those of the radiolabeled lipid metabolites in plasma are C_{L5}, V_{L5}. The release rate of the model drug out of the liposomes within the plasma and tissue compartments is given by k_r and k_T; transport of free dye to and from the tissue compartment is given by k_{12} and k_{21}; capture of liposomes by the liver is given by k_R; transport of free dye and metabolized-labeled lipid from the liver to the plasma is given by k and k_L; elimination of free dye and metabolites is given by k_e and k_{e_2}; diffusion of free dye, encapsulated dye and lipid into and out of the tumor is given by λ_1, λ_2, and λ_3. (b) the algorithm structure of the pharmacokinetic model. Dashed-line loops with arrows denote the iterative process of calculation which is repeated until all conditions are satisfied. Solid lines with arrows connecting imaging data and pharmacokinetic parameters are inner-subroutines which are applied to calculate the corresponding pharmacokinetic parameters for each iteration.

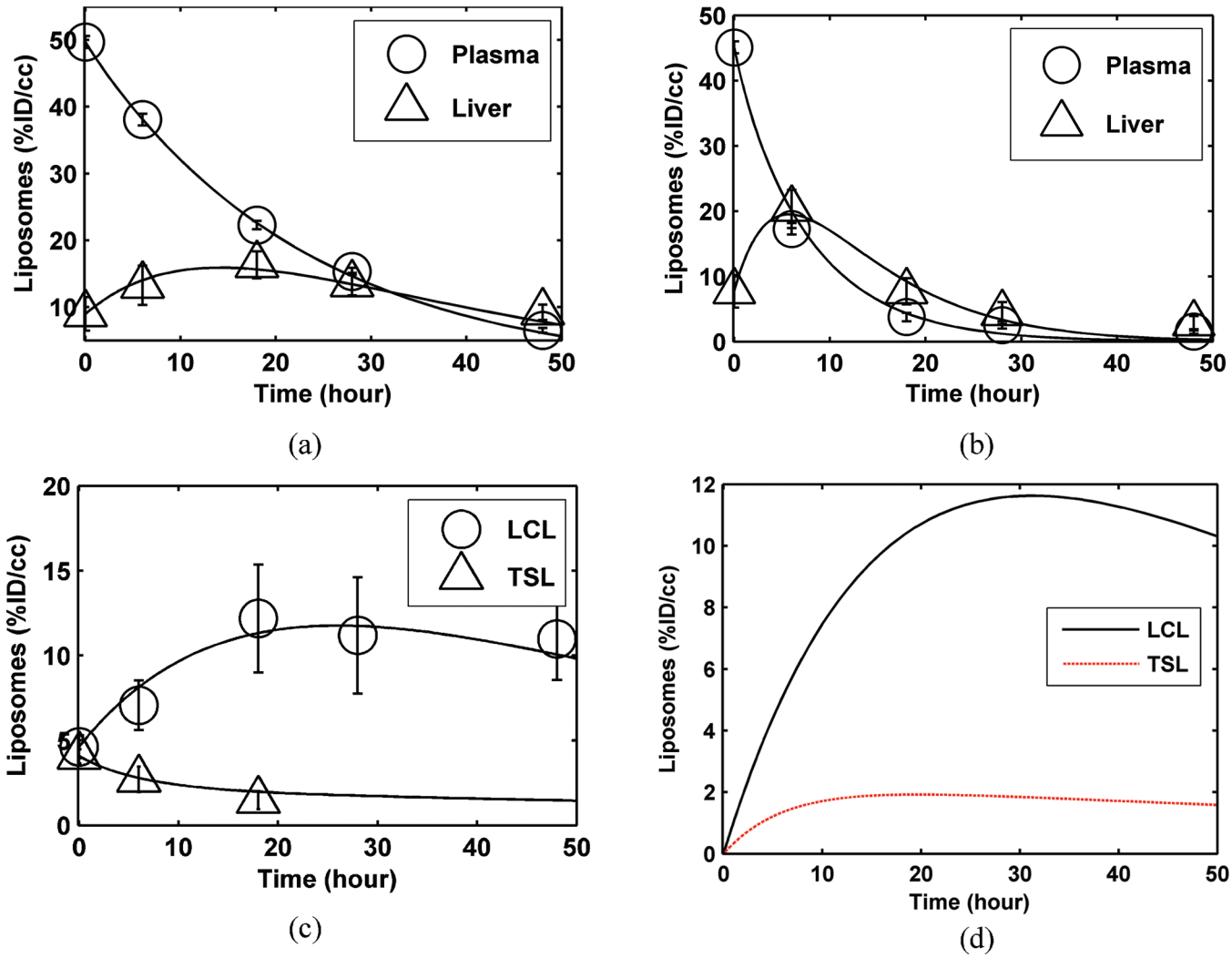

Figure 3. Micro-PET measurements (circle or triangle markers with errors bars) and corresponding model predictions (continuous or dashed lines) of the liposome concentration in plasma, liver, and tumor for different liposomal formulations. (a) LCL concentration in plasma and liver; (b) TSL concentration in plasma and liver; (c) liposome concentration in tumor for LCLs and TSLs, including liposomes in vessels within the tumor tissue; (d) the predicted concentration of the extravasated liposome in tumor interstitium for LCLs and TSLs. Length of the error bar is twice the acquired data standard deviation.

2(a). The pharmacokinetics within the plasma, tumor and liver compartments are explicitly measured and described by the model. For the purpose of the model, all other tissues are lumped within the tissue compartment. The particle size and our experimental data suggest that inclusion of the tissue compartment is necessary only for the free fluorophore. Because the mechanics and rate of the convection across the vessel wall are unknown, we used the transport constant to the tumor, λ (h^{-1}), to describe the apparent permeability including effects of the mass transport due to convection and diffusion, which is similar to the method used by Dreher et al.[28] The transport constant to the tumor, λ, is defined as the total mass transport rate (J_s) per unit tumor volume (V) and unit difference in concentration between tumor and plasma (ΔC), as in eq 7.

$$\lambda = \left(\frac{J_s/V}{\Delta C}\right)_{J_V \neq 0} \tag{7}$$

where J_V denotes the net fluid flux. Therefore, the mass conservation of the liposome and fluorophore in the whole body leads to the following differential equations:

$$C'_{\mathrm{L}} = -k_{\mathrm{R}}C_{\mathrm{L}} - \lambda_3\frac{V_{\mathrm{L}_3}}{V_{\mathrm{L}}}(C_{\mathrm{L}} - C_{\mathrm{L}_3});\ C'_{\mathrm{L}_3} = \lambda_3(C_{\mathrm{L}} - C_{\mathrm{L}_3})$$

$$C'_{\mathrm{L}_4} = k_{\mathrm{R}}\frac{V_{\mathrm{L}}}{V_{\mathrm{L}_4}}C_{\mathrm{L}} - k_{\mathrm{L}}C_{\mathrm{L}_4};\ C'_{\mathrm{L}_5} = k_{\mathrm{L}}\frac{V_{\mathrm{L}_4}}{V_{\mathrm{L}_5}}C_{\mathrm{L}_4} - k_{\mathrm{e}_2}C_{\mathrm{L}_5}$$

$$C'_{\mathrm{F}} = k_{\mathrm{r}}\frac{V_{\mathrm{E}}}{V_{\mathrm{F}}}C_{\mathrm{E}} + k\frac{V_R}{V_{\mathrm{F}}}C_{\mathrm{R}} + k_{21}\frac{V_{\mathrm{F}_2}}{V_{\mathrm{F}}}C_{\mathrm{F}_2} - k_{12}C_{\mathrm{F}} - k_{\mathrm{e}}C_{\mathrm{F}} - \lambda_1\frac{V_{\mathrm{F}_3}}{V_{\mathrm{F}}}(C_{\mathrm{F}} - C_{\mathrm{F}_3})$$

$$C'_{\mathrm{E}} = -(k_{\mathrm{R}} + k_{\mathrm{r}})C_{\mathrm{E}} - \lambda_2\frac{V_{\mathrm{E}_3}}{V_{\mathrm{E}}}(C_{\mathrm{E}} - C_{\mathrm{E}_3})$$

$$C'_{\mathrm{R}} = k_{\mathrm{R}}\frac{V_{\mathrm{E}}}{V_{\mathrm{R}}}C_{\mathrm{E}} - kC_{\mathrm{R}};\ C'_{\mathrm{F}_2} = k_{12}\frac{V_{\mathrm{F}}}{V_{\mathrm{F}_2}}C_{\mathrm{F}} - k_{21}C_{\mathrm{F}_2}$$

$$C'_{\mathrm{F}_3} = \lambda_1(C_{\mathrm{F}} - C_{\mathrm{F}_3});\ C'_{\mathrm{E}_3} = \lambda_2(C_{\mathrm{E}} - C_{\mathrm{E}_3}) \tag{8}$$

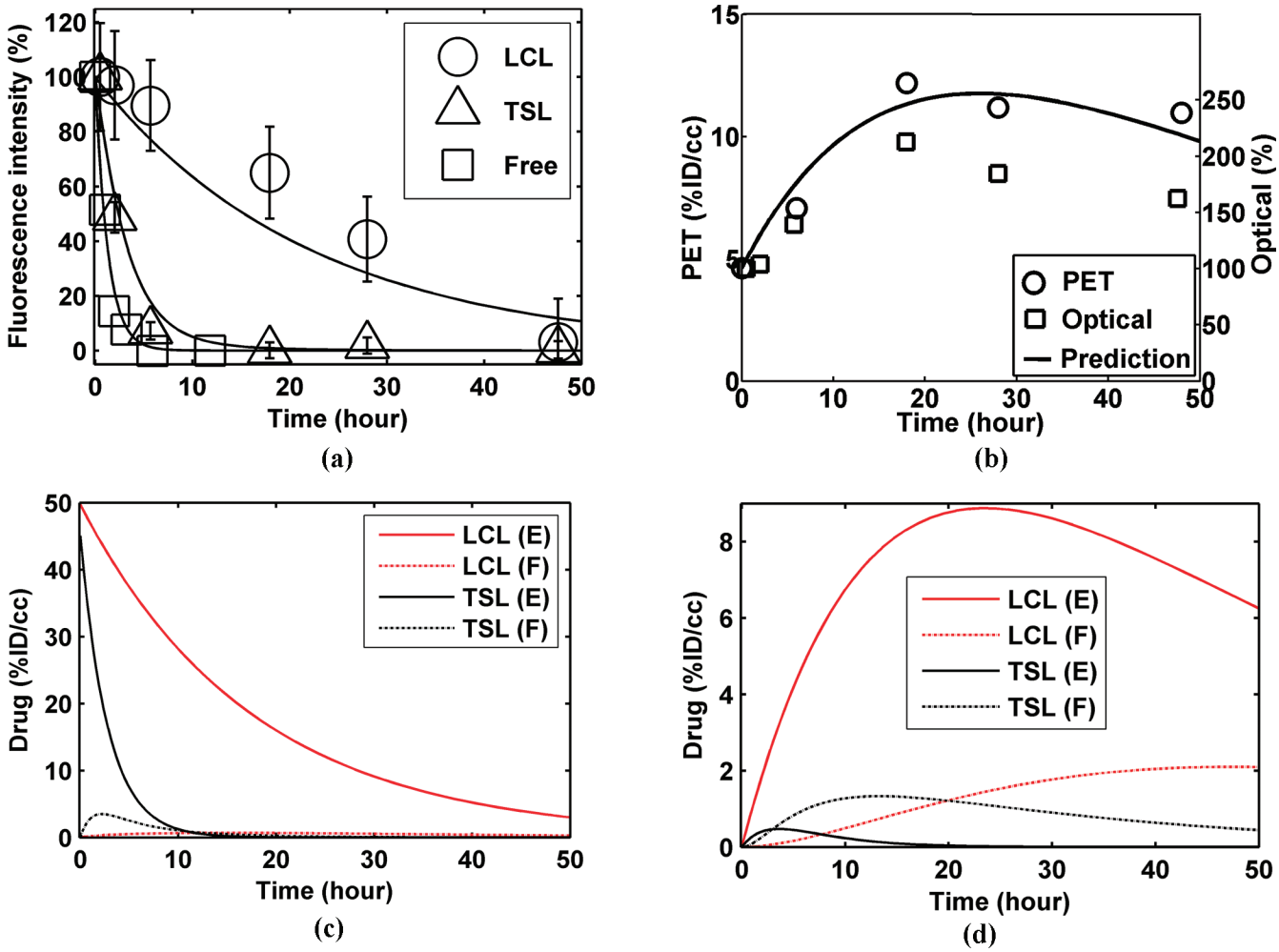

Figure 4. (a) and (b): Fluorescence intensity (markers with error bars) and corresponding model predictions (continuous or dashed lines) for the liposome-encapsulated fluorescent probe SIDA in plasma and tumor. The fluorescence intensity has been background-subtracted and normalized by the initial imaging intensity after the liposomes are administered. (a) In plasma. (b) LCL-SIDA images in tumor. (c) The predicted dye concentration in plasma, where the "E" denotes the encapsulated dye and the "F" denotes the released and free dye. (d) The predicted dye concentration in the tumor interstitium. Length of error bar is twice the acquired data standard deviation.

where λ_1, λ_2 and λ_3 refer to the transport constant to the tumor for the free drug, encapsulated drug and liposomes in the tumor compartment, respectively. The initial distribution phase of the liposome after injection is very fast and is neglected in the current calculation. For each experimental subject, eqs 4−6 and 8 were solved simultaneously and the solutions were optimized to fit all optical and PET data within all ROIs. For each data set, PET data were first applied to calculate a subset of parameters; then iterative processing was applied to all optical and PET measurements and parameters, see illustration in Figure 2(b). A MATLAB code was developed, and the residual was minimized using the nonlinear least-squares regression method. Statistical analysis was performed using a two-tailed Student *t*-test, and statistical significance was set at $p < 0.05$.

Results

After tail vein injection of liposomes, the particles are rapidly distributed in the vascular compartment. The liposome shell and the model drug are then tracked *in vivo* in real time (Figure 1), and PET measurements are first used to assess the PK of the shell. The difference between the plasma volume and the liposome distribution volume is small and is neglected in this analysis.[38] Based on the average weight of the mouse (∼22 g), the volumes of distribution for LCL and TSL as well as their metabolites are calculated to be ∼2.2 mL. The average tumor weight is ∼1 g, and the volume of distribution for the tumor is ∼0.1 mL. Over time, the particles accumulate in the liver and the distribution volume for LCL and TSL in liver is estimated based on the

(37) Wu, N. Z.; Braun, R. D.; Gaber, M. H.; Lin, G. M.; ONg, E. T.; Shan, S. Q.; Papahadjopoulos, D.; Dewhirst, M. W. Simultaneous measurement of liposome extravasation and content release in tumors. *Microcirculation—London* **1997**, *4* (1), 83–101.

(38) Allen, T. M.; Hansen, C. B.; Demenezes, D. E. L. Pharmacokinetics of Long-Circulating Liposomes. *Adv. Drug Delivery Rev.* **1995**, *16* (2−3), 267–284.

Table 1. Pharmacokinetic Parameters for Free and Liposomal Drug

(a) Distribution Volume for Liposomes and Liposomal Drug (mL)

V_L	V_{L_3}	V_{L_4}	V_{L_5}	V_E	V_{E_3}	V_R
2.2	0.1	2.5 (2.0)	2.2	2.2	0.1	2.5 (2.0)

(b) Kinetic Parameters for Free Drug

k_e, (h^{-1})	k_{12}, (h^{-1})	k_{21}, (h^{-1})	V_F, (mL)	V_{F_2}, (mL)	V_{F_3}, (mL)
0.77	0.0037	0.28	4.3	2.2	0.1

(c) Kinetic Parameters for Liposomes (h^{-1})[a]

		k_R	k_L	λ_3	k_r
LCL	m	0.046	0.056	0.021	0.003
	δ	0.005	0.032	0.006	0.014
	N	5	3	8	3
TSL	m	0.189	0.130	0.008	0.200
	δ	0.066	0.025	0.003	0.172
	N	3	3	6	3

[a] $m \pm \delta$: 95% confidence interval. N: subject number.

micro-PET measurements using the proposed model, leading to 2.5 mL for LCL and 2.0 mL for TSL. The distribution volume values used in calculation are summarized in Table 1.

The key predicted pharmacokinetic parameters are also summarized in Table 1. Radioactivity in the plasma after 48 h is 5.37% ID/cm^3 and 0.02% ID/cm^3 for LCL and TSL, respectively. For LCL, the 95% confidence interval for the mean transport constants of the liposomes and their metabolites to and from the liver, k_R and k_L, is 0.046 ± 0.005 h^{-1} and 0.056 ± 0.032 h^{-1}, respectively; each is significantly smaller than the liposome metabolite elimination constant ($k_{e_2} = 0.77$ h^{-1}, which is assumed to equal k_e for simplicity). Over the duration of the study, the plasma half-life for LCL and TSL is ~15.4 and ~5.4 h, respectively (Figure 3(a) and Figure 3(b)).

Circulating liposomes are primarily metabolized by the RES, where after injection the radioactivity in the liver is observed to increase gradually before declining. The model predicts that the peak concentration and the time to the peak in the liver are 19.5% ID/cm^3 at 5.6 h and 15.9% ID/cm^3 at 14.7 h for TSL and LCL, respectively, Figure 3(a) and Figure 3(b).

For the Met-1 tumor model, the PET data and analysis predict that the liposome transport constant to the tumor interstitium, λ_3, for the LCL and TSL systems is 0.021 ± 0.006 (h^{-1}) and 0.008 ± 0.003 (h^{-1}), respectively, with 95% confidence. LCL accumulate in tumor up to 11.76% ID/cm^3, peaking at 25.7 h after administration, while TSL concentration slowly decreases to 0.26% ID/cm^3 at 50.0 h after administration (Figure 3(c,d)).

Optical data are applied to estimate vehicle stability, described by the release constant of drug out of the liposomes, k_r, in Table 1. For encapsulated SIDA, the distribution volume in plasma is assumed to be equal to that of the liposomes. For free SIDA, the molecular size (<1 nm) is much smaller than that of the liposomes (~100 nm) and the estimated distribution volume for free SIDA is 4.3 mL, similar to the distribution volume reported for cisplatin. The experimental and predicted optical intensity for free and encapsulated SIDA in plasma are plotted in Figure 4(a), where the predicted values of the drug release constant k_r are 0.003 ± 0.014 h^{-1} and 0.200 ± 0.172 h^{-1} for LCL and TSL. Thus, the hydrophilic dye stably circulates within the LCL for the 48 h of our study, whereas the dye is released and cleared rapidly after the injection of TSL (Figure 4(b)).

Based on the pharmacokinetic parameters, the predicted drug concentration in plasma and the accumulated drug concentration in the tumor interstitium are plotted in Figure 4(c) and Figure 4(d). At 50 h after injection, the total drug concentration in plasma for LCL is 3.29% ID/cm^3 while that for TSL is ~0. In contrast, the free drug concentration in plasma following injection of LCL is ~0 and the peak free drug concentration in plasma following TSL injection is 3.5% ID/cm^3 at 2.1 h after injection.

The drug gradually accumulates in the tumor, peaks and then decreases for both carriers (Figure 4(d)). The peak value of the encapsulated drug concentration in the tumor interstitium for the TSL is 0.47% ID/cm^3 at 3.7 h after administration; the peak level for the LCL is 8.88% ID/cm^3 at 23.2 h after administration (Figure 4(d)). The peak value of the free drug concentration in the tumor interstitium is predicted to be 1.33% ID/cm^3 at 13.3 h and 2.09% ID/cm^3 at 47.5 h after administration for the TSL and LCL, respectively. Following the injection of LCL, the normalized area under the concentration−time curve (AUC) of total drug in the plasma and tumor (calculated from % ID/cm^3 over 50 h) is ~5.5-fold and 9-fold greater than following injection of TSL (Figure 5(a) and Figure 5(b)). However, the difference between the two formulation in the *free* drug AUC in plasma or tumor (Figure 5(c) and Figure 5(d)) is much smaller than the difference in *total* drug (Figure 5(a) and Figure 5(b)).

Discussion and Conclusions

PET and optical imaging were combined to yield the pharmacokinetic parameters for long and short circulating particles and to estimate the vascular permeability within tumors. PET estimates of tracer concentration within a tumor, liver and plasma are quantitative and have previously been validated through well counts, providing estimates of the tracer circulation, elimination and transport from plasma to liver. As expected, we find that these values are significantly changed by the incorporation of a lysolipid or cholesterol. We hypothesize that such measurements will be useful in the optimization of future temperature-sensitive particles.

The results here predict that in the absence of heating, the peak concentration and area under the curve for the encapsulated drug in tumor interstitium is ~19-fold and 9-fold greater following the administration of long circulating particles as compared with temperature sensitive particles. However, the peak value of free drug within the tumor interstitium varies only by 2-fold. In the interpretation of

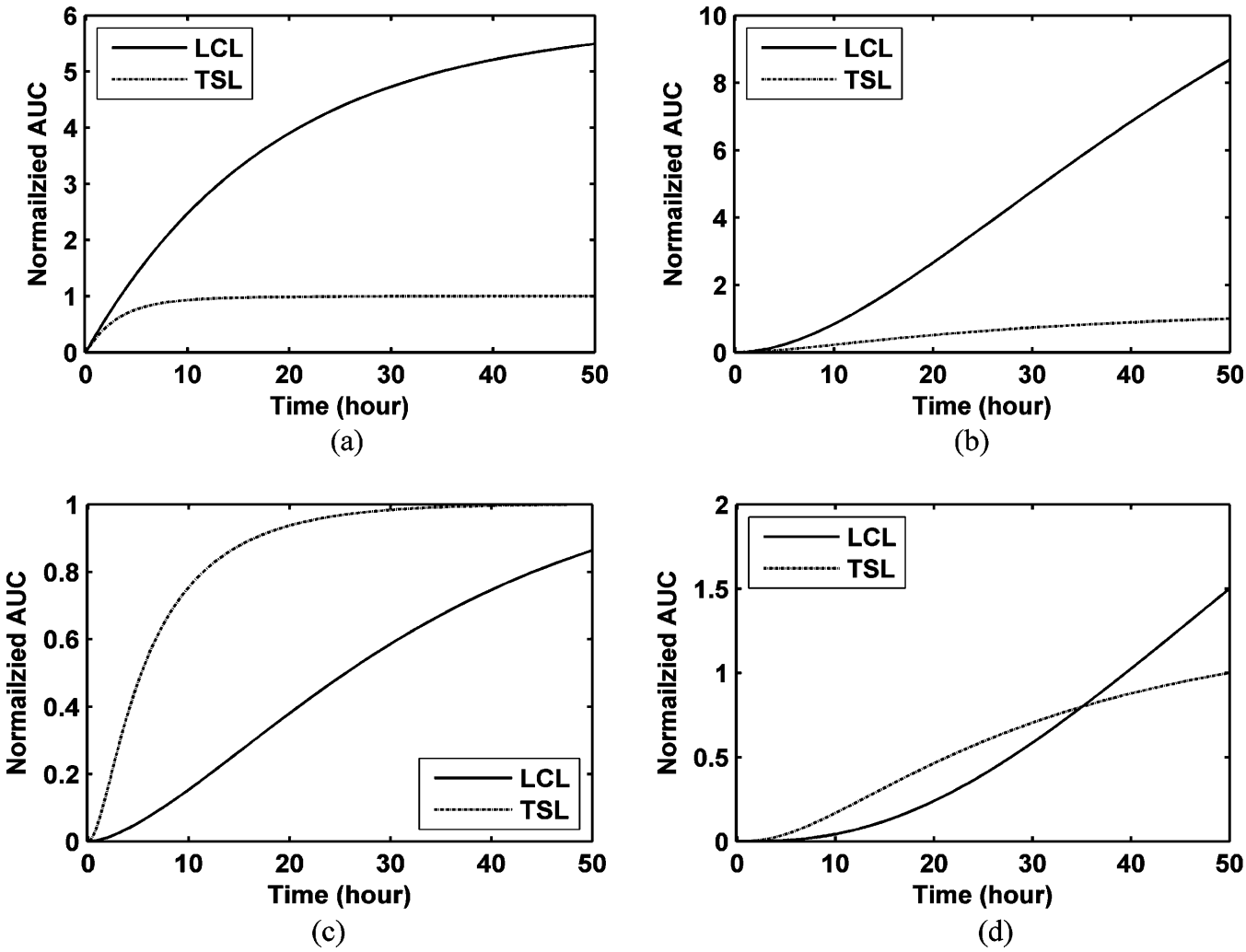

Figure 5. Predicted area under the concentration−time curve (AUC) of the drug carried by LCLs and TSLs. (a) Total drug in plasma; (b) total drug in tumor; (c) free drug in plasma; (d) free drug in tumor. AUCs are normalized by the corresponding AUC value for TSLs at 50 h after administration.

our PK parameters, it is important to recognize that we have not included the effect of temperature—instead, here we have considered only the PK of LCL and TSL without heat. If TSL are locally heated at the time of injection, as in refs 1, 9, 39, accumulation of the drug at the tumor site will be altered. The resulting PK can be evaluated with the methods employed here recognizing that each thermal dose and plan will change the resulting accumulation—significantly greater fractions of dose may reach the tumor than those predicted here. The evaluation of the native PK of the drug and particle is also important, however, since leakage of drug from the carrier can occur rapidly in all regions of the body. Based on the predicted release constant of drug out of the liposomes k_r, the drug release percent ($R\%$) over time can be obtained. For TSL, $R\% = e^{-k_r t}$ leads to 3.3% and 9.5% drug release at $t = 5$ and 30 min after administration, respectively, which agrees with measured data for TSL.[40] Accordingly, at $t =$ 10 and 15 h after administration, $R\%$ would reach 86.5% and 95.0%. Thus, the off-target accumulation of drugs such as doxorubicin in the heart or kidney may not be significantly changed by encapsulation in particles with a high value of k_r and this accumulation will ultimately limit the dose of particles injected.[9,39] Ideally, a future particle design might combine long circulation with induced release in the interstitium in the region of interest.

In order to simplify the model, calculation of the transport constant to the tumor, λ (h^{-1}), is based on the total mass transport rate per unit tumor volume and unit concentration difference between tumor and plasma. This definition differs from the diffusional or apparent permeability, P_{ad} (cm/s), which is commonly used by physiologists.[27,28] The relationship between λ (h^{-1}) and P_{ad} (cm/s) is

(39) Ponce, A. M.; Viglianti, B. L.; Yu, D. H.; Yarmolenko, P. S.; Michelich, C. R.; Woo, J.; Bally, M. B.; Dewhirst, M. W. Magnetic resonance imaging of temperature-sensitive liposome release: Drug dose painting and antitumor effects. *J. Natl. Cancer Inst.* **2007**, *99* (1), 53–63.

(40) Anyarambhatla, G. R.; Needham, D. Enhancement of the phase transition permeability of DPPC liposomes by incorporation of MPPC: A new temperature-sensitive liposome for use with mild hyperthermia. *J. Liposome Res.* **1999**, *9* (4), 491–506.

$$P_{ad} = \frac{V}{A}\lambda = \frac{D_0}{4\eta}\lambda \quad (9)$$

where V is the volume of the tumor, A is the total vascular surface area in the tumor, D_0 is the mean diameter of blood vessels in tumor, and η is the plasma volume fraction in tumor. Assuming the plasma volume fraction in the tumor is 5% and mean blood vessel diameter in tumor is 15 μm, the apparent permeability, P_{ad} corresponding to values of λ in Table 1 is 4.37×10^{-8} and 1.67×10^{-8} cm/s for the LCL and TSL, respectively, which is similar to the reported permeability values for hydrophilic solutes larger than 35 Å.[27]

The addition of an optical probe within the particle core serves several purposes. The stability of the drug within the delivery vehicle can be assessed in real time. Further, the stability of the radiotracer within the particle is validated by correlating these independent measurements of long circulating particles. We find some limitations in the use of the encapsulated optical probe for quantitative measurements. First, nonlinearity of optical measurements for a highly concentrated fluorophore results in a nonlinear relationship between optical efficiency and volume fraction. As a result, for the LCL, we do not quantify dye concentration at early time points after injection. Further, due to multiple scattering and attenuation, optical measurements cannot be compared between different organs; instead, values obtained for each organ should be compared across measurements or subjects.

Abbreviations Used

DPPC, 1,2-dipalmitoyl-*sn*-glycero-3-phosphocholine; MPPC, monopalmitoylphosphatidylcholine or 1-palmitoyl-2-hydroxy-*sn*-glycero-3-phosphocholine; HSPC, hydrogenated soy L-α-phosphatidylcholine; DSPE-PEG2K, 1,2-distearoyl-*sn*-glycero-3-phosphoethanolamine-*N*-[methoxy(polyethylene glycol)-2000]; BAT lipid, 6-[*p*-(bromoacetamido)benzyl]-1,4,8,11-tetraazacyclotetradecane-*N*,*N*′,*N*″,*N*‴-tetraacetic acid.

Acknowledgment. We appreciate the support of NIH CA 103828 and 112356.

MP900122J